Journal of Physical Chemistry C

Manuscript ID: jp-2023-01452v.R1

Toward Improved Anodic Stability of Ether-Based Electrolytes for Rechargeable Magnesium Batteries

Toshihiko Mandai[1,2*], Masaru Yao[3], Keitaro Sodeyama[2,3], Akiko Kagatsume[1], Yoshitaka Tateyama[1,2], and Hiroaki Imai[4]

[1]Center for Green Research on Energy and Environmental Materials, National Institute for Materials Science (NIMS), 1-1 Namiki, Tsukuba, Ibaraki 305-0044, Japan

[2]Center for Advanced Battery Collaboration, National Institute for Materials Science (NIMS), 1-1 Namiki, Tsukuba, Ibaraki 305-0044, Japan

[3]Research Institute of Electrochemical Energy, Department of Energy and Environment, National Institute of Advanced Industrial Science and Technology (AIST), 1-8-31 Midorigaoka, Ikeda, Osaka 563-8577, Japan

[4]Department of Applied Chemistry, Faculty of Science and Technology, Keio University, 3-14-1 Hiyoshi, Kohoku, Yokohama 223-8522, Japan

*Corresponding author footnote

Mail: MANDAI.Toshihiko@nims.go.jp TEL: +81-29-860-4464

Abstract

Rechargeable magnesium batteries (RMBs) are one of the promising energy-storage technologies for sustainable energy storage due to the abundant resources and intrinsically remarkable energy-storage properties of magnesium metal. However, to compete with alternative technologies, such as present lithium-ion batteries, there is a need to improve their energy density. One of the approaches to accomplish the above demand is to use high-voltage cathodes. The poor anodic stability of the current ether-based electrolytes compatible with magnesium metal anodes limits their working voltage and the choice of electrode materials. In this study, we explored different organic solvent-based electrolytes to design anodically-stable ether-based electrolyte solutions for RMB applications. Through the comprehensive experimental and computational surveys, we found that the intrinsic electrochemical/chemical stabilities against magnesium metal and the well-balanced solvating ability were necessary to achieve the desired functionality. Based on this knowledge, we designed and synthesized glyme-analogs bearing trifluoroalkyl groups. Consequently, we developed anodically-stable electrolytes that support electrochemical magnesium deposition/dissolution by combining suitable fluorinated-glyme-based solvents with appropriate conducting salts. These electrolytes showed a remarkable anodic limit of 4.4 V *vs*. Mg^{2+}/Mg (the highest ever reported to the best of our knowledge) and effectively suppressed the undesired corrosion of Al current collectors. However, these electrolytes could not be applied to RMBs with high-voltage oxide-based cathodes. Fragility against oxide-based cathodes caused undesired catalytic decomposition of the fluorinated solvents during charging.

Keywords: Electrolyte, ether, anodic stability, fluorination, magnesium battery

Introduction

The invention of rechargeable batteries is one of the greatest achievements of modern times. Lithium-ion batteries have led to significant changes and technological innovations in society, and their impact on industrial and social structures is immeasurable. However, to achieve sustainable development worldwide and improve societal well-being, the development of large-scale energy-storage technologies that are environmentally friendly is strongly recommended. Rechargeable batteries that use magnesium metal anodes are a promising option to meet these demands, as magnesium is abundant in nature, cost-effective, and has high specific/volumetric capacities, as well as inherent stability against ambient atmosphere.[1,2] Additionally, the less dendritic-growth nature of magnesium metal anodes upon repeated electrochemical deposition/dissolution cycling is desirable for safe battery operation, compared to conventional lithium metal anodes often experience fatal dendritic-growth issues.[3–5] Thus, rechargeable magnesium batteries (RMBs) have attracted considerable attention, and various fascinating electrode and electrolyte materials have been developed to realize RMBs with comparable or greater energy densities than present lithium-ion batteries.

Combining high-capacity cathodes, such as air (O_2) and sulfur, with high-capacity anodes, such as lithium metal, silicon, and low-dimensional carbon materials, is the current mainstream for research and development in both industry and academia when it comes to lithium-based batteries.[6–9] These cathode-active materials are believed to be promising for enhancing the energy densities of RMBs. However, the sluggish reversibility of O_2-related species and the substantially low working voltage of sulfur species make it extremely challenging to achieve reversible and high-energy densities for magnesium batteries.[10–12] Consequently, straightforward approaches, such as high-voltage transition metal oxides, appear more feasible for materializing high-energy-density RMBs.[13,14] According to the energy density calculator,[15] "realistic" RMBs that take into account the weight and volume of all battery components, including cathodes, anodes, current collectors, separators, electrolytes, tabs, tab-leads, films, and free space, can achieve *ca*. 300 Wh kg^{-1} and 600 Wh L^{-1} when a working voltage of 2.8 V and the discharge capacity of 270 mAh g^{-1} (based on the mass of cathode-

active materials) are reached. However, to realize such batteries, electrolytes that support electrochemical reactions at both magnesium metal anodes and high-voltage cathodes need to be developed. Conventional electrolyte solutions applicable to 4 V-class lithium-ion batteries, such as carbonates, nitriles, and sulphones, do not support fundamental interfacial reactions at magnesium anodes.[16,17] Due to the reductive nature of magnesium metal, most constituents of conventional electrolytes readily react with magnesium chemically, and the resulting passivation layer strongly hinders the diffusion of Mg^{2+} at [magnesium metal anode | electrolyte] interfaces.

The limited combinations of electrolyte salts and solvents allow reversible electrochemical deposition/dissolution of magnesium metal. Ethers are one of the representative cathodically-stable solvents. Indeed, ether solvents are typically used in major electrolyte solutions for electrochemical magnesium deposition/dissolution.[2,16] The ethereal solutions of magnesium bis(trifluoromethanesulfonyl)amide ($Mg[TFSA]_2$) support somewhat reversible magnesium deposition/dissolution with modest Coulombic efficiencies.[18,19] To improve interfacial kinetics and suppress passivation in modest electrolytes, organic/inorganic halide species and strong Lewis acids are effective additives for magnesium deposition/dissolution,[20,21] although their mechanisms and functions are still controversial. However, these additives, mostly halide species, often have drawbacks, such as insufficient anodic stability, high corrosivity, and incompatibility with typical transition-metal-oxide cathodes.[22] To avoid these drawbacks due to additives, different approaches have been developed to enhance and induce reversible magnesium electrochemistry, including the modification of solvation sheath by dual solvents and artificial interfacial engineering for modestly active and even inactive electrolytes, respectively.[23–28] The former solvent approach is particularly practical with respect to the practical battery materialization, as the surface chemistry and morphology of the metallic anode systems would successively change during cycling. Recent studies into designing electrolyte materials based on the solution chemistry have achieved promising $Mg[TFSA]_2$-based electrolytes by combining ether and certain organic solvents.[23,25–27] The dual-solvent systems would offer better electrochemical characteristics than those composed of ether solvents solely by modulating solvation states and solution structures. These successes challenge the established theory that magnesium is only compatible with ethereal solvents and could pave the way for high-energy-density

RMBs with suitable electrolytes that simultaneously support reversible magnesium electrochemistry and sufficient anodic stability.

To identify the appropriate electrolyte formulations for high-energy-density RMBs that use high-voltage oxide-based cathodes, we conducted a new study on organic solvent-based single-solvent electrolytes. We examined their electrochemical magnesium deposition/dissolution activities and anodic limits in a comprehensive survey that combined systematic experimental investigation with first-principle calculations. Our findings confirm that intrinsic electrochemical/chemical stabilities against magnesium metal anodes and well-balanced solvating ability are essential for achieving the solvents that allow electrochemical magnesium deposition/dissolution. We also discovered that single-solvent electrolytes composed solely of the second solvents in previously reported dual-electrolyte systems did not support electrochemical magnesium deposition. Based on these findings, we attempted to introduce the functional groups in the ether architectures to improve the anodic stability without spoiling the favorable characteristics of ethers. Our optimal electrolyte exhibited moderate compatibility with magnesium metal anodes and excellent anodic stability.

Methods

Materials. The electrolyte salts of $Mg[Z(HFIP)_4]_2$ (Z = B or Al; HFIP = hexafluoroisopropoxyl) were synthesized using established procedures.[29,30] Commercially available, anhydrous solvents were used as received, while solvents whose water contents could not be guaranteed by the suppliers were dried by vacuum distillation over suitable pre-drying agents and treated with activated 3-Å molecular sieves and then stored in an Ar-filled glovebox. A series of electrolyte solutions were prepared by dissolving predetermined amounts of the salts in the studied organic solvents, and the solutions were vigorously stirred at 30 °C overnight in an Ar-filled glovebox (O_2, H_2O <1 ppm, UNICO). As the solutions of $Mg[Z(HFIP)_4]_2$ dissolved in conventional glyme (G*n*; *n* indicates number of the ethylene oxide unit) solvents showed the highest ionic conductivities at around 0.3 mol dm^{-3} irrespective of the coordination center of the anions and the number of ethylene oxide units of glymes,[30] the

concentrations of the solutions were fixed at that concentration unless otherwise noted. The water content of the prepared electrolytes was measured at <30 ppm by Karl Fischer titration.

Synthesis of fluorinated ethers. A series of fluorinated glymes bearing trifluoromethyl (TFM), 2,2,2-trifluoroethyl (TFE), and 3,3,3-trifluoropropyl (TFP) groups were synthesized following the conventional Williamson reactions[31,32] or the modified silver-mediated direct *O*-trifluoromethylation,[33] depending on the molecular structure of the introduced functional groups. The chemical structure and purities of the synthesized fluorinated ethers were identified by ^{1}H, ^{13}C, and ^{19}F nuclear magnetic resonance (NMR) spectroscopy. Detailed synthetic conditions and analytical data are provided in the Supporting Information (Figures S1–S4).

GnTFM (*n* = 2 or 3): The silver-mediated direct *O*-trifluoromethylation was adopted to synthesize trifluoromethoxy-type glyme-analogs from the corresponding oligoethylene glycols. The obtained crude product was purified by silica-gel column chromatography, followed by vacuum distillation to yield colorless liquid products at approximately 20% yield. As outstanding battery performance was observed when applying G*n*TFM to lithium-based batteries, the detailed synthetic procedure for G*n*TFM will be provided in our subsequent study.

GnTFE (*n* = 2 or 3): Another anhydrous tetrahydrofuran (THF) solution of 2,2,2-trifluoroethanol was added dropwise to an ice-cold suspension of NaH (60% dispersion in paraffin oil, 4.0 equiv.) in anhydrous THF at 0°C. After vigorous stirring at ambient temperature (22±2°C) for 2 h, the anhydrous THF solution of the corresponding oligoethylene glycol bis(*p*-toluenesulfonate) precursors were added slowly at 0°C, followed by refluxing with continuous stirring for 24 h. The reaction mixture was cooled to ambient temperature; then, 10 wt% aqueous solution of NH_4Cl was added to quench the excess sodium alkoxide. The aqueous phase was extracted with ethyl acetate, and the combined organic phase was washed with deionized water and saturated NaCl aqueous solution every three times. The solution was dehydrated with anhydrous $MgSO_4$ and subsequently concentrated using a rotary evaporator. The crude product was purified by vacuum distillation to yield the colorless liquid at >80% yield.

GnTFP (*n* = 2 or 3): The same procedure as G*n*TFE synthesis was adopted using 3,3,3-trifluoropropanol instead of 2,2,2-trifluoroethanol. The resulting crude product was purified by vacuum distillation to yield the colorless liquid at approximately 40% yield.

Transport properties. The transport properties, such as ionic conductivity, liquid density, and viscosity, were evaluated for various fluorinated ether-based and some selected electrolytes. The ionic conductivities were measured using the complex impedance method with an impedance analyzer (VMP3, Biologic). A commercial cell equipped with two platinized platinum electrodes (CT-57101B, TOA DKK Corporation) was used for the impedance measurements. The liquid densities and viscosities were measured using a kinematic viscometer (SVM3001, Anton Paar GmbH). All the standard deviations in the experimental values were within ±3% of the average.

Electrochemistry. The electrochemical magnesium deposition/dissolution activities of a series of electrolyte solutions were assessed by cyclic voltammetry (CV) using a typical three-electrode beaker-type cell. A Pt disk (φ3 mm, BAS) and pure Mg ribbon (FUJIFILM Wako Chemicals) were used as working and counter electrodes, respectively, while an Ag^+/Ag electrode was employed as a reference for CV measurements. The Ag^+/Ag reference was fabricated and calibrated according to the previously reported procedure.[29,34] The magnesium deposits were obtained by potentiostatic polarization of a Pt disk working electrode at –1.0 V *vs*. Mg^{2+}/Mg in 0.3 mol dm^{-3} $Mg[Al(HFIP)_4]_2$/G2TFE-G3TFE (in 50:50 vol%). The anodic corrosion tests of Al foil current collectors were conducted to investigate the corrosive nature of the prepared electrolytes. Three-electrode cells were assembled using the Al current collectors (φ16 mm) as a working electrode, a porous glass fiber as a separator (GF/A, Whatman, *t* = 0.26 mm), mechanically polished magnesium foil (99.94%, homemade, φ16 mm, *t* = 0.04 mm) as a counter electrode,[35] and an Mg^{2+}/Mg electrode as a reference. The Mg^{2+}/Mg reference was fabricated by soaking a mechanically polished Mg wire (99.999%, Nilaco) in 0.3 mol dm^{-3} $Mg[Al(HFIP)_4]_2$/G2, where electrochemical magnesium deposition-dissolution taking place almost at 0 V *vs*. Mg^{2+}/Mg.[30] The working electrodes were polarized in the fluorinated ether-based electrolyte solutions at the predetermined potentiostatic conditions for 16 h at ambient temperature. The

aforementioned electrochemical measurements were conducted using an electrochemical analyzer HSV-110 (Hokuto-Denko Corporation) located in an Ar-filled glovebox.

The discharge-charge cycling tests were performed using two- or three-electrode setup cells. The nanostructure-engineered $MgMn_2O_4$ served as a cathode-active material.[36] The cathode formulations comprised $MgMn_2O_4$: multiwall carbon nanotube: polyvinylidene difluoride = 92: 4: 4 in weight ratio. The mixture was dispersed in *N*-methylpyrrolidone to obtain a slurry and then coated on an Al current collector. The dried cathode sheets were compressed by a roll press, cut into a circular shape with a diameter of 16 mm (the average mass loading was fixed at 3 mg cm^{-2}), followed by heat treatment under a high vacuum at 80 °C for 24 h to completely remove adhered water and remaining NMP. The cells were assembled using a $MgMn_2O_4$ cathode, GF/A separator immersed in certain fluorinated and non-fluorinated electrolytes, and mechanically polished magnesium foil. For the three-electrode setups, an Mg^{2+}/Mg reference was used. Galvanostatic discharge-charge tests were performed using a battery-testing system (Hokuto Denko, HJ1001SD8C). The current density of 10 mA g^{-1} and a cut-off voltage of +0.2 and +4.0 V were adopted. All discharge-charge tests were performed at 30 °C. Each test was repeated at least three times separately to ensure experimental reproducibility.

Chemical and Morphological Analysis. The electrodeposited magnesium metal and polarized current collectors were examined using scanning electron microscopy (SEM; JSM-7800F, JEOL) and subsequently characterized by energy dispersive X-ray (EDX) spectroscopy. X-ray photoelectron spectroscopy (XPS; VersaProbe II, ULVAC-PHI) was also used to characterize the current collectors. XPS measurements were conducted with an Al Kα X-ray source under a base pressure of less than 6.7×10^{-8} Pa. The binding energy of the obtained spectra was calibrated using the C 1s peak from sp^2-hybridized carbon at 284.5 eV as a reference. To prepare the samples, all the impurities were removed by washing with anhydrous ethylene glycol dimethyl ether and the samples were dried under a high vacuum at ambient temperature. The samples were then placed in an airtight chamber and transferred for SEM–EDX analysis or XPS measurements without any exposure to air.

Calculation. The DFT calculations were conducted using the Gaussian 16 software package[37] at the M06-2X/aug-cc-pVTZ level, taking into account the solvent effect with the SMD model.[38] The permittivity of each solvent was used for the calculations, and the dielectric constant was set to 7.23 for the fluorinated and sulfonated glyme-analogs, which corresponds to the non-modified glyme. The zero-point energy and counterpoise correction were not included in the calculations. The oxidation energy (ionization potential (IP) in solvent) was determined by calculating the energy difference between the relaxed cation and neutral states, whereas the reduction energy (electron affinity (EA) in solvent was determined by calculating the energy difference between the relaxed neutral and anion states. The binding energy (BD) of the solvent with Mg^{2+} was calculated by $BD = E_{Mg} + E_{solvent} - E_{solvate}$, where E_{Mg}, $E_{solvent}$, and $E_{solvate}$ represent the energies of Mg^{2+}, solvent, and solvate, respectively.

Results & Discussions

Revisiting the solvent survey for Mg deposition-dissolution: As described in the introduction part, reversible electrochemical magnesium deposition-dissolution are only allowed in limited ethereal solutions. However, recent studies have identified a promising avenue for developing magnesium battery electrolyte compositions. Certain ether-based dual solution systems of $MgCl_2$ and $Mg[N(CF_3SO_3)_2]_2$, such as ether-sulfone,[23,24] ether-amine,[25,26] and ether-phosphate,[27] have demonstrated favorable electrochemical characteristics. However, achieving reversible magnesium deposition-dissolution in non-ethereal single-solvent electrolyte solutions remains a challenging task.[24] The second solvents in these solutions play a specific role as chelating agents to kick the counter anions in the first Mg^{2+}-solvation shell away, stabilizing the isolated counter anions and subsequently the [magnesium metal | electrolyte] interface.[23,25] These dual-solvent systems impart complicated solution states as mutual interactions among three Lewis basic components, including the ether, second solvents, and counter anions, which compete with attractive interactions of the Lewis bases with Lewis acidic Mg^{2+}. To simplify the solution and interfacial chemistries and identify the solvents that are compatible with magnesium metals, this study surveyed a single salt-solvent system with $Mg[Z(HFIP)_4]_2$ as a conducting salt. The coordination ability of this anion is considerably small;[30,39,40]

thus, Mg^{2+}-anion interactions would be negligible. A large variety of commercially available solvents, including ethers, nitriles, amines, amides, carbonates, acid esters (acetates, phosphates, and borates), sulfoxides, sulfites, sulfones, ketones, alcohols were studied. All primitive CV results are summarized in the Supporting Information (Figures S5–S8). To avoid scattering focuses, this study discusses some specific results for $Mg[B(HFIP)_4]_2$-based electrolytes.

Figure 1 shows that the choice of electrolyte solvents determines the electrochemical activity for magnesium deposition-dissolution. Most ethereal solutions are intrinsically compatible with magnesium metal; thus, allowing reversible magnesium deposition-dissolution, except for dipropylene glycol dimethyl ether solution, which requires substantially large polarization to proceed deposition and dissolution reactions. Although the reason for this observation is not clear, it is possible that the coordination structures of Mg^{2+} surrounded by propylene oxide units, $O(CH_2CH_2CH_2O)_n$, may cause such inferior electrochemical characteristics.

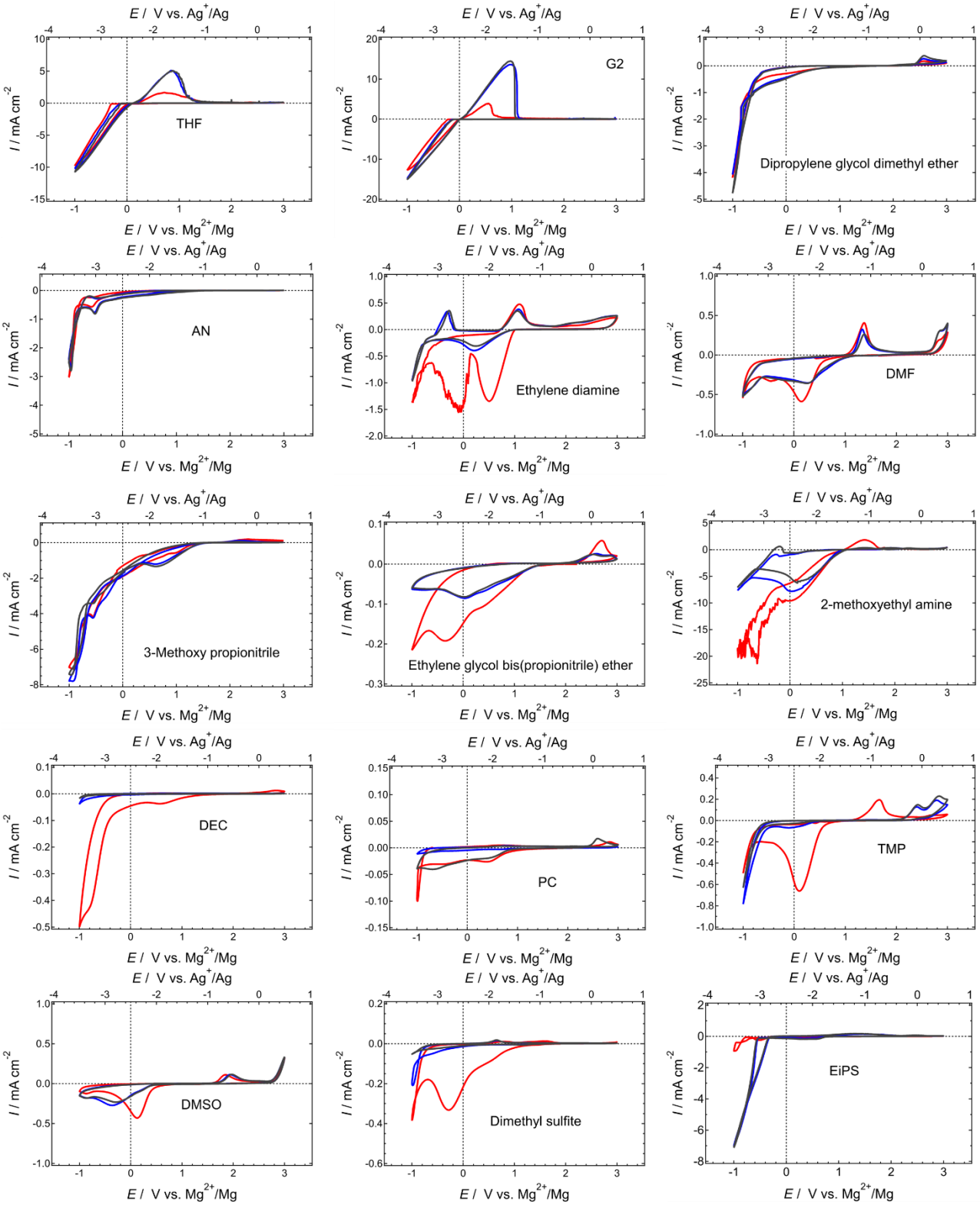

Figure 1. Cyclic voltammograms of Pt working electrodes recorded in a series of $Mg[B(HFIP)_4]_2$-based electrolyte solutions at a scan rate of 10 mV s^{-1} at 30 °C. Red, blue, and gray curves indicate the 1st, 5th, and 10th cycles, respectively. THF, tetrahydrofuran; G1, monoglyme; G2, diglyme; AN, acetonitrile; DMF, dimethyl formamide; DEC, diethyl carbonate; PC, propylene carbonate; TMP, trimethylphosphate; EiPS, ethyl isopropyl sulfone.

Reduction current responses can be observed for the electrolytes using the solvents containing nitrogen-based functional groups, such as nitrile, amine, and amide. These responses are attributed to electrolyte side reactions, such as reductive decomposition and the corresponding re-oxidation of reduction products, despite their occurrence at approximately the ideal equilibrium potential of Mg^{2+}/Mg.[41] Solid deposits were not detected on the working electrodes after certain potentiostatic polarization in these electrolytes; however, unidentified sticky compounds were found. It is worth noting that the hybrid solvents of ether and nitrile, like 3-methoxypropionitrile and ethylene glycol bis(propionitrile) ether, are inactive for magnesium deposition-dissolution, indicating that the detrimental effects of nitrile on magnesium would evolve preferentially. The electrolyte solutions of 2-methoxyethylamine, a kind of hybrid solvent of ether and amide, exhibit irregular CV profiles. This family has recently been reported to be an effective second solvents for enhancing the electrochemical activity of ethereal solutions of $Mg(TFSA)_2$ by modifying the solvation environment of Mg^{2+}.[25] Somewhat coupled cathodic and anodic responses can be found at approximately –0.7 and –0.3 V vs. Mg^{2+}/Mg. The electrolyte solution of ethylenediamine, a non-ethereal counterpart of the 2-methoxyethylamine, also showed similar coupled responses in the same range, –0.7 and –0.3 V, in addition to another couple at +0.5 and +1.0 V vs. Mg^{2+}/Mg. As these electrolytes are inactive for magnesium deposition-dissolution due to the absence of deposits of magnesium metal even after CV and potentiostatic measurements, the observed redox couples should come from somewhat reversible redox reactions of the solvent, not the desired magnesium deposition-dissolution reactions.

Previously reported studies have noted the presence of peaks in carbonate-based electrolytes that cannot be attributed to either magnesium deposition or dissolution.[16] It is worth noting that the current densities of the observed CV profiles for the carbonate-based electrolytes are considerably smaller than those observed in nitrogen-based electrolytes. The salt was well dissociated in carbonate- and nitrogen-based solvents, as evidenced by the ionic conductivity measurements (Figure S9), suggesting that the interface formed by carbonate-derived electrolytes may be highly insulating. Such a carbonate-derived interface may be formed during the initial cathodic process. The reductive decomposition of the carbonate group took place at approximately +1.0 V vs. Mg^{2+}/Mg, as all studied carbonate-based electrolytes have similar cathodic current profiles for initial scans. A similar

mechanism can be observed in other acid-ester solutions, such as acetate and phosphate. However, the studied salt was not dissolved in borates, possibly due to the extremely weak coordinating ability of borate esters.

In contrast to the electrolyte solutions containing sulfoxide, sulfite, and cyclic sulfone (referred to as sulfolane), which are inactive electrochemically for magnesium deposition-dissolution, the ethyl isopropyl sulfone (EiPS)-based electrolyte exhibits a different CV profile. This electrolyte shows a large reduction current, which is readily assignable to the magnesium deposition reaction. Similar curves can be obtained for the EiPS electrolyte containing $Mg[Al(HFIP)_4]_2$ as a conducting salt (Figure S10), further supporting the modest compatibility of the solvent against magnesium metal. The deposits obtained from the EiPS electrolyte consisted of magnesium and certain amounts of impurity elements originating from the decomposition of the electrolyte. Unfortunately, the oxidation currents corresponding to magnesium dissolution were considerably small or negligible, although the EiPS solution allows magnesium deposition. The surface passivation of magnesium deposits due to the cathodic decomposition of the electrolyte constituents may impede the dissolution of the deposits during the reverse scans. The reversibility of magnesium deposition-dissolution of dialkyl sulfone-based electrolyte solutions can be improved by adding ethers. As shown in Figure S11, somewhat reversible responses can be observed during the anodic scan for the CV profiles of the dialkyl sulfone-glyme dual-solvent electrolytes.

In summary, typical glymes are only the solvents that possess remarkable compatibility with reductive magnesium metal electrodes and good solvating ability toward various magnesium salts. Meanwhile, the other single organic solvents would impede reversible electrochemical magnesium deposition-dissolution reactions mainly due to their interfacial instability. Mixing certain solvents with glymes may improve the compatibility of the resulting dual-solvent electrolytes against magnesium metal compared to the single non-ethereal electrolytes. However, the relatively inferior compatibility of these solvents against magnesium would impart insufficient performance. Moreover, the anodic stability of these dual-solvent electrolyte solutions would not be able to be improved as anodically unstable solvents, in most cases ethers or amines, would be oxidized preferentially during the anodic scan. To gain anodically stabile ethers, the introduction of electron-withdrawing groups into the

molecular structures of ethers by covalent bonding has been proposed. The inductive effect through a σ-bond by electron-withdrawing groups results in polarizing anodically fragile ether oxygen moieties, making the compounds anodically stable. This synthetic approach worked well for ethers functionalized by fluoroalkyl groups to enhance the anodic stability of the resulting ethers without losing the good compatibility against lithium metal.[42,43] Based on the similar chemical nature of lithium and magnesium metals, the same approach should be adoptable in developing anodically-stable ethereal electrolytes for magnesium batteries. In this study, a computational survey has been conducted to synthesize compounds to specify the electron-withdrawing functional groups that are potentially compatible with magnesium metal-negative electrodes.

Computational survey toward feasible ether structures: Oxidation and reduction energies of the representative solvent compounds with different functional groups are summarized in Table 1. The binding energies of the molecules against magnesium ions are also included in the table. The energy levels of the highest occupied and lowest unoccupied molecular orbitals, HOMO and LUMO, respectively, are often referred to as measures of oxidative and reductive stabilities of compounds. However, these energy levels do not necessarily reflect the corresponding stabilities due to the lack of the principle of the energy differences between reactants and products.[44] In this study, to make a reliable prediction of anodically-stable ether structures, we adopted adiabatic ionization potential (IP) and electron affinity (EA) based on the relevant electron-transfer processes to estimate the oxidative and reductive stabilities of compounds, respectively. The detailed computational studies on the quantitative evaluation of the redox and solvation characteristics of major liquid electrolytes will be reported in a separate paper.

Table 1. Oxidation and reduction energies of a series of representative organic solvents. The dielectric constants (ε_r) and binding energies with Mg^{2+} were also included.

Solvents	ε_r	Oxidation energy / eV		Reduction energy / eV		Binding energy with Mg^{2+} / eV
		HOMO	Adiabatic IP	LUMO	Adiabatic EA	
EC	89.8	–10.306	–8.535	–0.012	–0.643	0.599
PC	66.1	–10.210	–8.360	–0.012	–0.603	0.647

DEC	2.82	–10.084	–8.891	–0.069	–0.007	2.052
GBL	39.0	–9.465	–8.020	–0.024	–0.850	0.835
THF	7.52	–8.564	–7.175	0.020	–0.266	1.242
AN	36.64	–10.947	–9.294	0.013	–0.494	1.085
DMF	38.3	–8.194	–6.613	0.011	–0.639	0.451
SL	43.4	–9.246	–7.754	0.010	–0.385	0.801
DMSO	47.2	–8.011	–6.406	0.058	–0.520	1.204
TMP	20.6	–10.070	–8.029	–0.075	–0.490	1.231
G1	7.30	–8.941	–7.844	0.016	–0.170	2.086
G2	7.23	–8.951	–7.006	–0.012	–0.169	2.987
G3	7.62	–8.956	–7.045	–0.027	–0.177	3.815

Footnote. EC, ethylene carbonate; PC, propylene carbonate; DEC, diethyl carbonate; GBL, γ-butyrolactone; THF, tetrahydrofuran; AN, acetonitrile; DMF, dimethyl formamide; SL, sulfolane; DMSO, dimethyl sulfoxide; TMP, trimethylphosphate; G1, monoglyme; G2, diglyme; G3, triglyme.

For magnesium battery applications, electrolytes must be stable against magnesium metal-negative electrodes. Therefore, reductive stabilities, namely, EAs, of the solvents are important parameters to be considered. As shown in Table 1, sulfone, sulfoxide, phosphate, and linear carbonate will be potential candidate groups for ether functionalization with respect to the EAs. Among them, sulfoxide must be excluded because of its poor oxidative stability (referred to as IP in Table 1). Unexpectedly, a linear carbonate, e.g., diethyl carbonate, is stable against reduction and oxidation, whereas cyclic carbonates are susceptible, especially against reduction. As demonstrated in Figure 1 and many preceding works, the electrochemical magnesium deposition does not occur in any carbonate-based electrolyte solutions. This discrepancy between computation and experimental may arise from not the electrochemical but chemical instability of carbonate groups against magnesium metal.[45] Indeed, an artificial interface that makes electrolyte components away from direct contact with magnesium metal enables reversible magnesium electrochemistry even in carbonate-based electrolytes.[28] In contrast to the sulfoxide and carbonate groups, the sulfone and phosphate groups are still fascinating because the corresponding solvents have shown certain adoptability against magnesium metals.[23,24,27] As expected from the computation on the sulfone molecule, the oxidative

stability would improve by combining glyme with sulfone without seriously spoiling the favorable reductive stability of ethers (Table 2). Figure S12 shows the corresponding chemical structures of sulfonated glyme-analogs. The number and position of the sulfonyl-group replacement on the ether oxygen atoms have a minor impact on the electrochemical stabilities.

Table 2. Oxidation and reduction energies and binding energies with Mg^{2+} of sulfonated and fluorinated-glyme analogs. The data of parent non-modified G2 were also included as a reference.

Solvents	Oxidation energy / eV		Reduction energy / eV		Binding energy with Mg^{2+} / eV
	HOMO	Adiabatic ionization potential	LUMO	Adiabatic electron affinity	
G2	–8.951	–7.006	–0.012	–0.169	2.987
G2-F1	–9.481	–8.091	–0.081	–0.372	1.572
G2-F2	–9.451	–8.448	–0.098	–0.366	1.830
G2-F3	–9.675	–8.341	–0.090	–0.296	1.663
G2-F4	–11.057	–9.844	–0.061	–0.276	0.486
G2-F5	–12.752	–10.078	0.104	–0.168	–0.681
G2-S1	–9.162	–7.937	–0.084	–0.360	2.119
G2-S2	–9.408	–7.974	–0.152	–0.418	3.003

Partial/full fluorination of hydrocarbons (H replacement by F) is also one rational approach for designing molecules with enhanced oxidative stability. To clarify the effect of fluorination on the electrochemical stabilities and solvating ability, fluorinated-glyme analogs were investigated systematically based on the G2 structure as a model system. These chemical structures are illustrated in Figure S12. The number and position of fluorination have a strong impact on the electrochemical stabilities (Table 2). The contribution of fluorination on the terminal methyl group to the reduction stability seems small, whereas that on the ethylene unit backbones is relatively large. A similar trend can be found for the oxidation stability sides. The difference in the degree of contribution of fluorination may arise in their molecular structures and the resulting extent of the impact of the inductive effect of fluorine atoms on the electronic states of the adjacent ether oxygen atoms. The

inductive effect through σ-bond is well-known to be diminished with distancing. Therefore, the inductive effect of each terminal CF_3 can affect the electronic state of the directly bonded single oxygen atom. However, the effect of fluorinated ethylene units will be provided on two adjacent ether oxygen atoms. Moreover, the inductive effect becomes prominent for the further or fully fluorinated cases, e.g., G2-F4 and G2-F5 (Table 2 and Figure S12), improving the oxidation stabilities. The perfluorination simultaneously diminishes the coordination ability of the solvents (Table 2). Based on the computational speculations, partly fluorinated-glyme analogs will be considered.

Unfortunately, any attempts of the isolation of the phosphonated glyme compounds from reaction mixtures failed, irrespective of the synthetic routes (i.e., esterification between an acid chloride and alcohol and exchange of alkoxide groups on the P atom), probably due to the comparable polarity/chemical characteristics of reagents, desired products, and by-products. In contrast, the introduction of sulfonyl groups in the glyme structures can be achieved under typical addition reactions using vinyl sulfone with corresponding ethylene glycol derivatives catalyzed by triphenylphosphine.[46] The introduction of fluorinated hydrocarbons in glyme structures is also achievable by conventional chemical reactions. By combining synthetic accessibility and electrochemical stabilities, sulfonated and fluorinated-glyme analogs are feasible ethereal solvents with enhanced oxidative stabilities.

Electrochemistry of fluorinated-ether-based electrolytes: According to the computational estimations, sulfonated and fluorinated-glyme analogs have been synthesized. It is worth noting that the sulfonated glyme-analogs are highly viscous irrespective of the position and number of introduced sulfonyl groups due to the strong inter and intramolecular interactions of sulfonyl groups. Although somewhat reversible electrochemical magnesium deposition and dissolution can be observed upon elevating the measurement temperature (Figure S13), we focused on the fluorinated-glyme analogs to avoid the effect of another dynamic factor on the electrochemical properties.

In addition to the electrochemical stabilities, the position of fluorination in the chemical structures of glyme-analogs has a dominant impact on the solvating abilities (Table 2). The solvating ability of solvent molecules is pivotal to achieving magnesium-ion-conductive electrolyte solutions. Indeed, one representative fluorinated oligoether 2,2,3,3-tetrafluoro-1,4-dimethoxybutane, which is

recently recognized as a promising ethereal solvent for high-voltage lithium metal batteries,[42] is incompatible with any studied magnesium salts as no clear solution can be obtained, whereas the $Mg[Z(HFIP)_4]_2$ salts are soluble in the non-fluorinated counterpart. Additionally, the magnesium salts as well as the corresponding lithium salts are not soluble in the perfluorinated G3 analog because of the inferior solvation ability of solvents induced by the direct fluorination on the ether backbone. To maintain the sufficient solvating ability against magnesium salts and enhance the anodic stability of glyme-analogs simultaneously, trifluoroalkyl groups, such as trifluoromethyl (TFM), 2,2,2-trifluoroethyl (TFE), and 3,3,3-trifluoropropyl (TFP), are substituted on both terminal methyl groups of glymes. These solvents are hereafter denoted as G*n*TFX, where *n* indicates the number of ethylene oxide units, and X is referred to as M (methyl), E (ethyl), or P (propyl). Their chemical structures are summarized in Scheme 1.

X	*n* = 2	*n* = 3
M	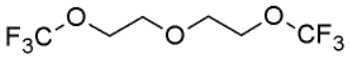	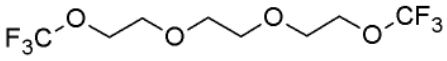
E	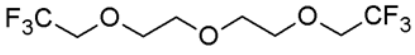	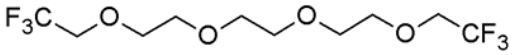
P	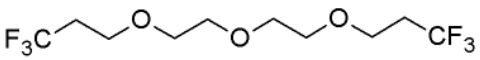	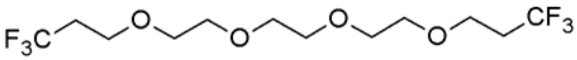

Scheme 1. Chemical structures of the synthesized fluorinated-glyme analogs G*n*TFX.

The solvation ability of these terminal fluorinated-glyme analogs G*n*TFX is also found to be alkyl-length dependent (Table S1). For ionic compounds, it is well understood that the balance of the binding energies between anion-cation and solvent-cation complexes is responsible for the solubility of ionic compounds in solvents. The binding energies of the solvent-Mg^{2+} complexes increase with distancing the CF_3 from the ether oxygen atoms (–O–) and with increasing the number of ethylene oxide units. The experimental results clearly reflect these trends that the $Mg[TFSA]_2$ and $Mg[Z(HFIP)_4]_2$ salts are insoluble in the G*n*TFM irrespective of the anion coordination center (Z) and

the number of ethylene oxide units *n*. $Mg[B(HFIP)_4]_2$ was scarcely soluble in G*n*TFP, soluble in part in G2TFE, but completely soluble in G3TFE at the concentration of 0.3 mol dm^{-3}, whereas the $Mg[Al(HFIP)_4]_2$ counterpart was soluble at the same concentration in all studied G*n*TFE and G*n*TFP. $Mg[TFSA]_2$ does not dissolve in any fluorinated-glyme analogs. For the binding energies of $[TFSA]^-$, $[B(HFIP)_4]^-$, $[Al(HFIP)_4]^-$, and G2TFX with Mg^{2+}, the values for [TFSA]-Mg^{2+} are substantially larger than G2TFX-Mg^{2+}, as summarized in Table S1. For the soluble cases, such as $Mg[Al(HFIP)_4]_2$ in G2TFE, the binding energies of solvent-Mg^{2+} are larger than those of anion-Mg^{2+} complexes. Although the greater binding energy for G2TFE-Mg^{2+} than $[B(HFIP)_4]$-Mg^{2+} suggests complicated competitions of interactions among the solvent, anion, and Mg^{2+} behind a salt solubility, the results illustrate that controlling the solvation ability of solvents by an appropriate chemical modification is crucial to achieve ion-conductive solutions with sufficient carrier-ion concentrations.

The primitive electrochemical magnesium deposition/dissolution characteristics of a series of fluorinated-glyme analogs-based electrolytes were evaluated by CV. The CV profiles of the saturated solution of $Mg[B(HFIP)_4]_2$ in G2TFP are displayed in Figure S14. As shown in Figures 2 and S14, all the electrolyte solutions containing the $Mg[B(HFIP)_4]_2$ conducting salt were unexpectedly inactive. The reduction currents can be observed at approximately 1 V vs. Mg^{2+}/Mg, suggesting undesired side reactions during the initial cathodic scan. In stark contrast, certain electrolyte solutions based on $Mg[Al(HFIP)_4]_2$, especially those incorporating G*n*TFE solvents, showed favorable electrochemical magnesium deposition/dissolution activities. In addition to the electrochemical activities, the solution states may be different between $Mg[Al(HFIP)_4]_2$- and $Mg[B(HFIP)_4]_2$-based solutions as the colorless solutions were obtained for $Mg[Al(HFIP)_4]_2$, while the solution color would turn brownish for $Mg[B(HFIP)_4]_2$ (Figure S15). This color change for $Mg[B(HFIP)_4]_2$ was induced by the decomposition of the anions, as evidenced by the corresponding ^1H NMR spectra shown in Figure 3. The peak assignable to $B(HFIP)_3$ molecules was obviously detected for the spectrum of the saturated $Mg[B(HFIP)_4]_2$/G2TFE solution, although the peak is absent for the parent salt and solvent. Due to the structural bulkiness of the HFIP group and the relatively short distance between B and O of HFIP, the crowded $[B(HFIP)_4]^-$ structure would be fragile.[47,48] DFT MD simulations on $Mg[B(HFIP)_4]_2$-ether solutions also suggested the decomposition of $[B(HFIP)_4]^-$ anion into $B(HFIP)_3$ and $[HFIP]^-$

(alkoxide) upon ion-pair formation.[30,49] The relatively strong solvation ability of $[B(HFIP)_4]^-$ than $[Al(HFIP)_4]^-$ can facilitate the undesired anion decomposition, consequently leading to the electrochemically inactive nature of the $Mg[B(HFIP)_4]_2$-based solutions. For the $Mg[Al(HFIP)_4]_2$/G2TFE solution in contrast, no peak assignable to $Al(HFIP)_3$ molecules is discernible in the corresponding spectrum, ensuring the superior structural stability of $[Al(HFIP)_4]^-$ owing to the relatively less crowded nature around Al.[48,50]

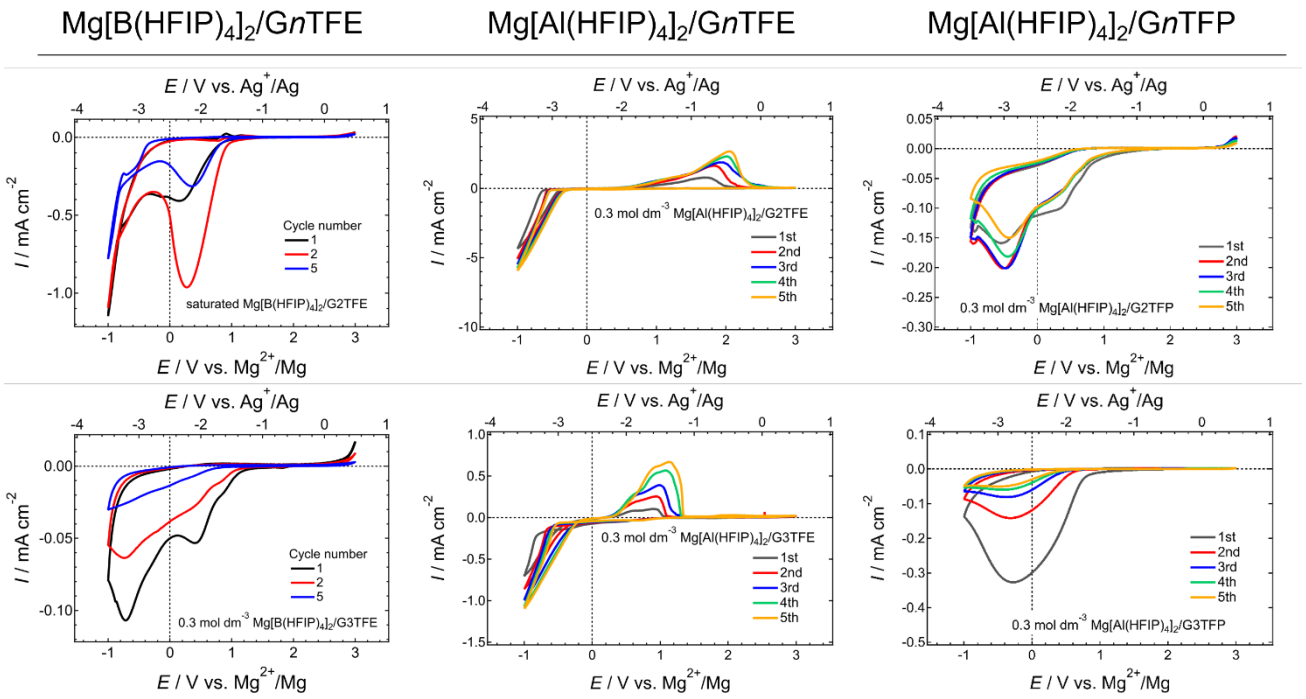

Figure 2. CV profiles of Pt working electrodes recorded in 0.3 mol dm^{-3} $Mg[Z(HFIP)_4]_2$ dissolved in G*n*TFE and G*n*TFP (Z = B and Al) at a scan rate of 10 mV s^{-1} at 30°C.

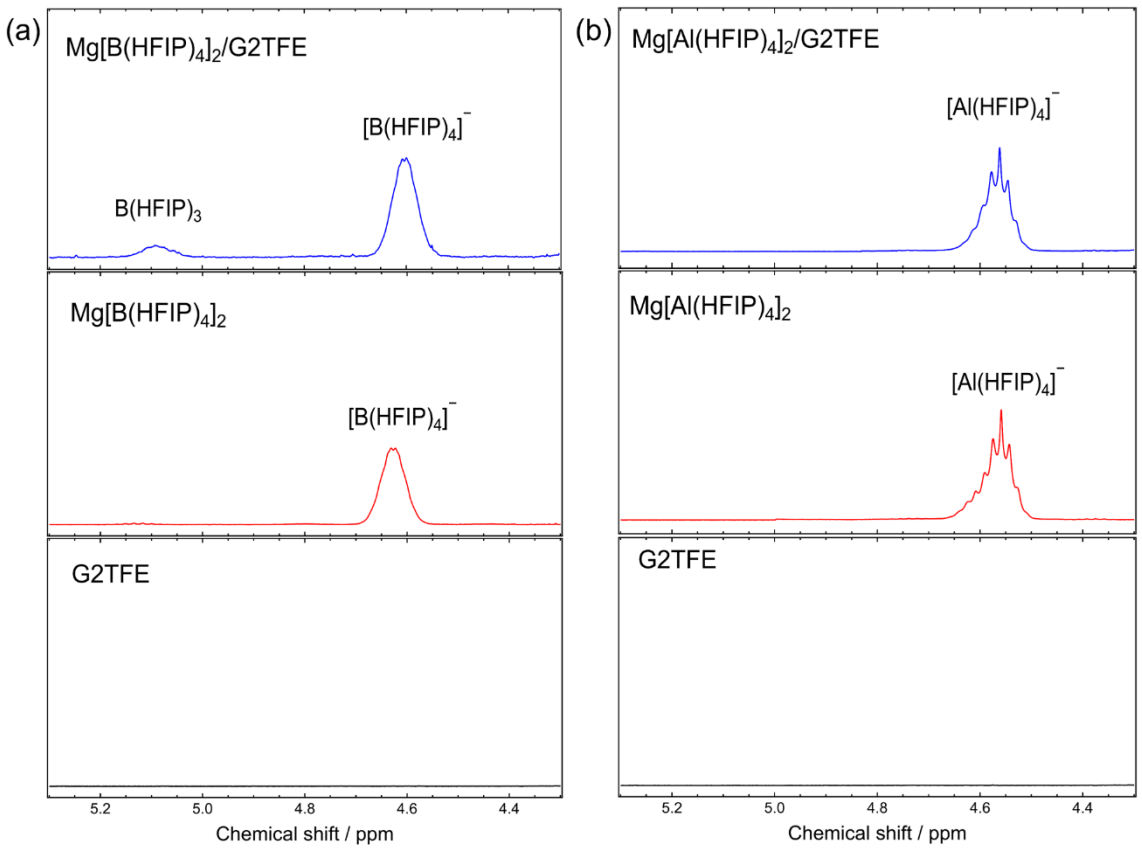

Figure 3. ^{1}H NMR spectra of the G2TFE solvent, Mg[Z(HFIP)$_4$]$_2$ salts, and Mg[Z(HFIP)$_4$]$_2$/G2TFE solutions. (a) Z = B, (b) Z = Al. The specific spectral range for [Z(HFIP)$_4$] and Z(HFIP)$_3$ were adopted.

The CV profiles of Mg[Al(HFIP)$_4$]$_2$/G*n*TFE vary depending on the number of ethylene oxide units *n* (Figure 2). The highest current densities for magnesium deposition/dissolution are achieved by dissolving Mg[Al(HFIP)$_4$]$_2$ into G2TFE. However, the G2TFE solutions simultaneously require greater overpotential than the corresponding G3TFE solutions. This dependence on the number of ethylene oxide units for the overpotential has also been observed in non-fluorinated conventional glyme-based electrolytes.[30] This difference in solvation structure and desolvation energies required for charge transfer at the [electrode | electrolyte] interface is likely the reason for this observation. The electrochemical performance can be improved by combining the G2TFE and G3TFE solvents. Figure S16 shows the CV profiles for the solutions with different mixing ratios of G2TFE and G3TFE and different salt concentrations. The optimal performance was achieved by mixing G2TFE and G3TFE in a 50:50 volume ratio at a salt concentration of 0.3 mol dm^{-3}. For the optimal electrolyte, the smallest overpotential (onset potential) combined with the moderate current density for magnesium

deposition/dissolution was observed (Figures 4a and 4b). Even with this optimal electrolyte solution, the electrochemical magnesium deposition/dissolution activity is still lower than that of the non-fluorinated counterpart. The lower ionic conductivities of the fluorinated electrolytes than those of the non-fluorinated may be responsible for the modest electrochemical activity (Figure S17).

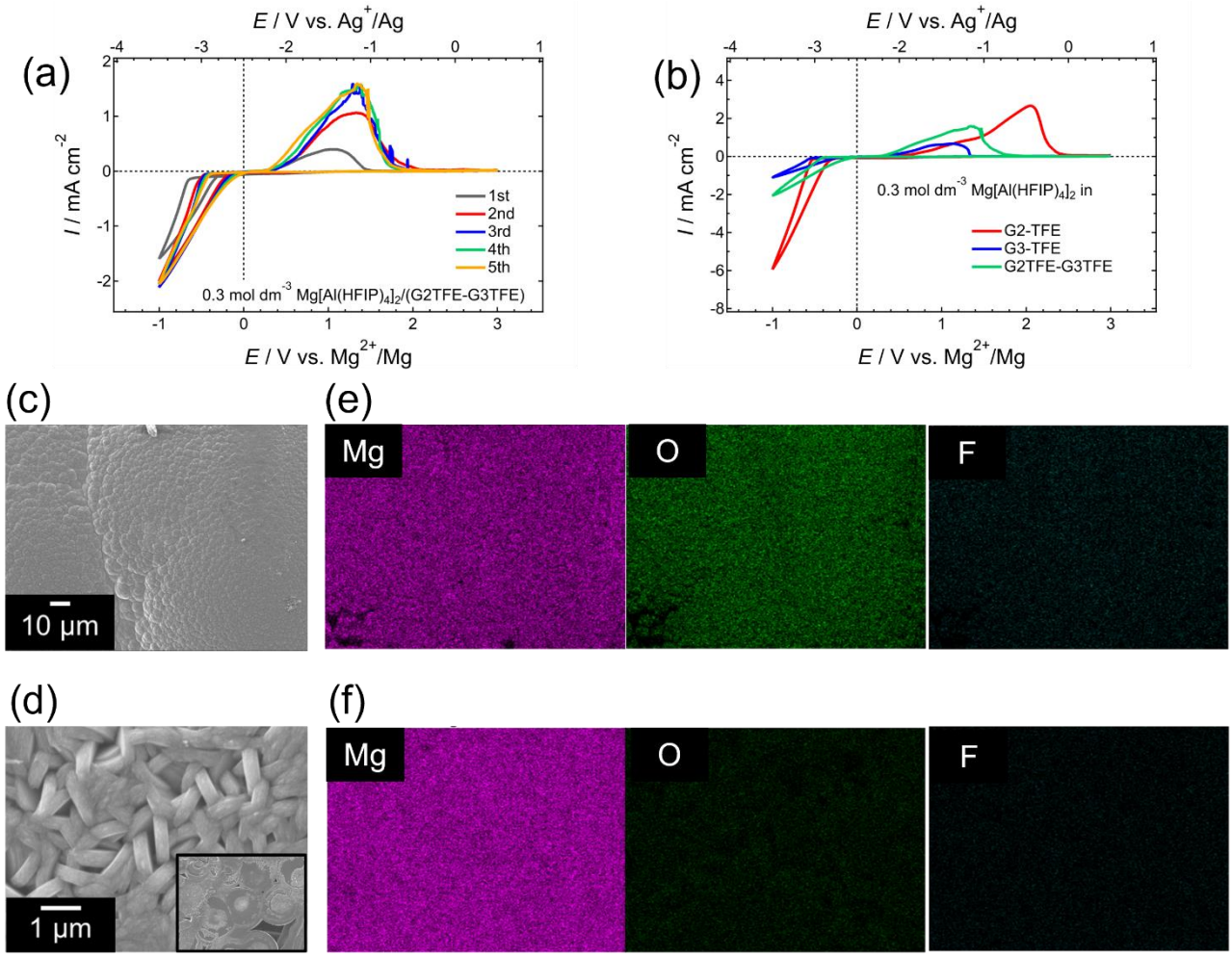

Figure 4. (a), (b) CV profiles of 0.3 mol dm^{-3} $Mg[Z(HFIP)_4]_2$ dissolved in G2TFE, G3TFE, and their mixtures. The SEM images and EDX mapping profiles of (c), (e) upper- and (d), and (f) bottom-surface of deposits obtained from the optimal electrolyte.

The deposits obtained from the optimal electrolyte by galvanostatic polarization were observed by SEM, and the results are shown in Figures 4c and 4d. A representative granular-shaped morphology was confirmed for the upper surface of deposits (Figure 4c). The fine rounded grains with a diameter of approximately 1 μm were agglomerated to be higher-ordered rounded particles. Such rounded magnesium deposits are typically found in $Mg[TFSA]_2$-based electrolytes.[18,19] However, the bottom-surface images support different morphological aspects (Figure 4d). The shape of the primary

particles was not rounded but rather angulated. The high-resolution image clearly indicated that the higher-ordered particles were composed of rectangular-shaped primary particles, except for certain areas that were presumably exposed to the electrolyte. A similar morphology of magnesium deposits can also be found for the ethereal solutions containing $MgCl_2$ and $LiPF_6$.[41] These observations strongly suggest that the crystalline magnesium can be deposited from the present electrolyte and the deposits would subsequently react with the electrolyte constituents. A larger amount of fluorine atoms, originating from the electrolyte decomposition, can be detected on the upper surface than on the bottom surface of deposits by the following elemental analyses (Figures 4e and 4f).

It is worth noting that the electrolyte solutions based on the G*n*TFP solvents exhibit low electrochemical activity for magnesium deposition/dissolution despite their good solvating ability (Figure 2 and Table S1). Although we do not have a clear explanation for these observations, it is possible that the fortified coordination of magnesium ions by fluorine atoms of the terminal trifluoromethyl group in G*n*TFP, in addition to the ether oxygen atoms, inhibits facile desolvation at the interface and electrochemical activity. Similar enhanced binding by side arms has been reported for complexation by lariat-crown ethers.[51]

The anodic stability of the fluorinated-ether-based electrolytes was examined by the linear sweep voltammetry (LSV) on Pt working electrodes with a scan rate of 1 mV s^{-1}. Expectedly, the anodic limits of the electrolytes were remarkably improved by employing the fluorinated-glyme analogs as a solvent (Figure 5). The anodic stability of the conventional ethereal electrolytes is limited by the oxidation of the ether solvents, at around 3.5-3.7 V vs. Mg^{2+}/Mg.[39,40,52] The potential, where the anodic current density of 0.05 mA cm^{-2} was observed, was shifted by about 0.7 V, from 3.7 to 4.4 V vs. Mg^{2+}/Mg, for our $Mg[Al(HFIP)_4]_2$/G*n*TFE against the non-fluorinated counterpart. To the best of our knowledge, this value, 4.4 V vs. Mg^{2+}/Mg, is the highest anodic limit among the ever-reported ether-based magnesium electrolytes. The introduction of trifluoroalkyl groups into glyme structures is certainly responsible for this favorable result.

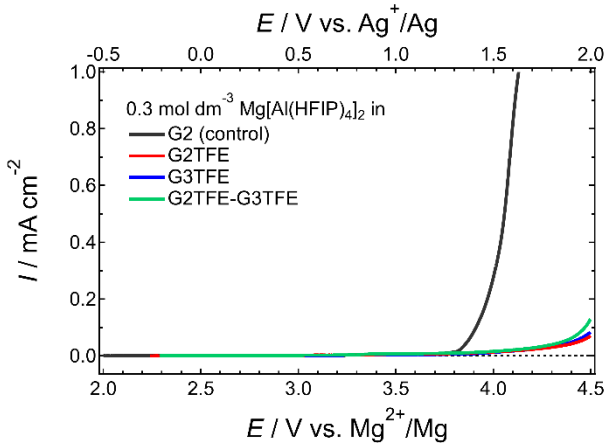

Figure 5. LSV profiles of Pt working electrodes recorded in 0.3 mol dm^{-3} $Mg[Al(HFIP)_4]_2$ dissolved in G*n*TFE (*n* = 2 and 3) at a scan rate of 1 mV s^{-1} at 30°C. The profile recorded in the non-fluorinated G2-based counterpart was also included as a control.

In summary, electrochemically-active and anodically-stable magnesium electrolyte solutions have successfully been developed. The high anodic stability of these electrolytes has the potential to enable the design of high-energy-density magnesium batteries using high-voltage cathode-active materials. However, our attempts to use these electrolytes in combination with oxide-based cathode-active materials have failed due to poor compatibility with fluorinated-glyme analogs. The next section discusses both the positive and negative aspects of these electrolytes in magnesium battery applications and lays the groundwork for future research on designing fascinating electrolyte materials.

Pros and Cons of fluorinated-glyme analogs-based electrolytes: As shown in Figure 5, the anodic stability was significantly improved upon substituting the terminal methyl groups into fluorinated alkyl groups of the glyme structures. Additionally, the fluorinated-glyme analogs-based electrolytes can effectively suppress the undesired corrosion of Al current collectors. The preceding studies have reported that corrosion of Al current collectors would take place at approximately 3.5 V by LSV; however, pitting corrosion can be detected on the Al surface by polarizing at 3.0 V for a longer period in the ethereal solutions of $Mg[Al(HFIP)_4]_2$.[39] The same results were obtained in this study for an Al current collector polarized for 16 h at the fixed cell voltage. The chronoamperograms of an Al current collector measured in the non-fluorinated $Mg[Al(HFIP)_4]_2$/G2 electrolyte are indicative of corrosion taking place, even at 3.0 V vs. Mg^{2+}/Mg (Figure 6a), although the LSV measurements indicated its

sufficient anodic stability over 3.5 V vs. Mg^{2+}/Mg on Pt. The following SEM observations support severe pitting corrosion of an Al current collector (Figure 6b). The depth profiles of Al 2p and F 1s XPS spectra suggested an organic–inorganic hybrid fluoride surface layer formation upon decomposition of the non-fluorinated electrolyte (Figures 6c and 6d). The inorganic aluminum fluoride films are beneficial to inhibit further dissolution of Al species into the electrolyte and consequently suppress the breakdown of the current collector in typical $LiPF_6$-based electrolytes for lithium-ion batteries.[53] However, such inorganic aluminum fluoride films do not work well in certain electrolytes, particularly containing $[TFSA]^-$ anions.[54] A similar chemistry on an Al current collector as [TFSA]-based electrolytes in lithium-ion batteries may apply to the present $Mg[Al(HFIP)_4]_2$-based electrolytes in magnesium batteries.

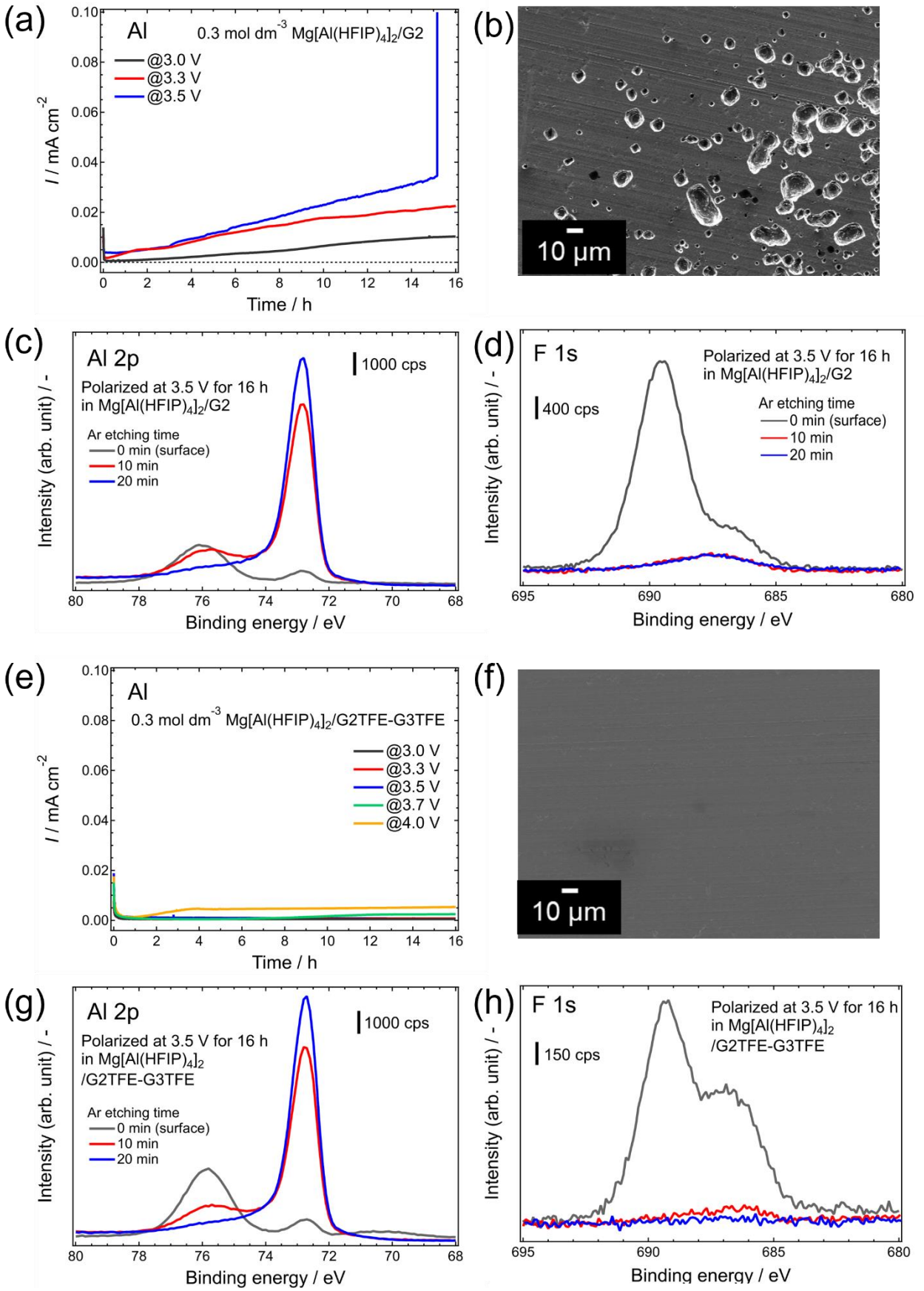

Figure 6. (a) and (e) The chronoamperograms of Al current collectors; (b) and (f) the SEM images, (c) and (g) Al 2p, and (d) and (h) F 1s spectra of the Al current collectors after static polarization at

3.5 V. The electrolyte solutions of 0.3 mol dm^{-3} $Mg[Al(HFIP)_4]_2$ dissolved in (a)-(d) G2 and (e)-(h) G2TFE-G3TFE were used.

In stark contrast, the corrosion of an Al current collector can effectively be ameliorated using fluorinated-glyme analogs-based electrolytes. As shown in Figure 6e, no anodic currents can be observed for an Al current collector polarized at 3.5 V vs. Mg^{2+}/Mg in $Mg[Al(HFIP)_4]_2$/G2TFE and $Mg[Al(HFIP)_4]_2$/G2TFE-G3TFE. Even at 4 V, a rapid breakdown of an Al current collector was suppressed, while continuous anodic currents, presumably attributed to the electrolyte decomposition, were observed. The SEM images of the Al current collectors after polarization also showed no visible evidence of Al corrosion (Figure 6f). The corresponding Al 2p and F 1s XPS profiles indicated an organic–inorganic hybrid fluoride layer formation on the surface of the polarized Al current collector, as well as the case using the non-fluorinated electrolyte (Figures 6g and 6h). However, the relative intensity of inorganic fluoride (Al-F, 686 eV) against organic fluoride (CF_n, 689 eV) is strong for the collectors polarized in the fluorinated-glyme-analogs-based electrolytes compared to that in the non-fluorinated counterpart, strongly suggesting suppressed dissolution of the inorganic fluoride layer and beneficial passivation of an Al current collector by fluorinated-glyme-analogs. The same passivation phenomena were observed for the fluorinated-ether-based lithium electrolyte systems.[42,43]

The battery cycling tests were conducted based on these advantageous properties of the fluorinated-glyme-analogs-based electrolytes for achieving high-voltage magnesium batteries using the spinel-type oxide-based cathodes, magnesium metal anodes, and developed electrolytes. Figure 7 shows the typical discharge-charge profiles of the two-electrode cells, including the profiles of the cell using non-fluorinated electrolytes. The OCV of the cells was decreased by 0.5 V using the fluorinated-glyme analogs-based electrolytes. This potential drop implies the passivation of magnesium anodes upon undesired side reactions with the electrolytes. The behavior of the initial discharge and subsequent charging is a clear reflection of the characteristics of electrolytes. When in contact with the electrolyte, the passivation of magnesium anodes results in a significant positive shift of the electrode potential of the anodes. This leads to inferior working voltage and discharge capacities for the cells using fluorinated-glyme analogs-based electrolytes. The discharge-charge measurements

using three-electrode setups, where an Mg^{2+}/Mg electrode was used as a reference, further support the unexpectedly large positive shift of the electrode potential of the magnesium electrode by approximately +0.7 V as an OCV against the reference (Figure S18). Moreover, the fluorinated electrolyte was found to be unstable against the $MgMn_2O_4$ cathode. The chronoamperograms of $MgMn_2O_4$ cathodes polarized in the fluorinated electrolyte (Figure S19) clearly indicated side reactions taking place even at 3.5 V vs. Mg^{2+}/Mg, lower potential than the anodic limit of the electrolytes. The catalytic activity of transition metal oxides would facilitate this electrolyte decomposition.[55,56]

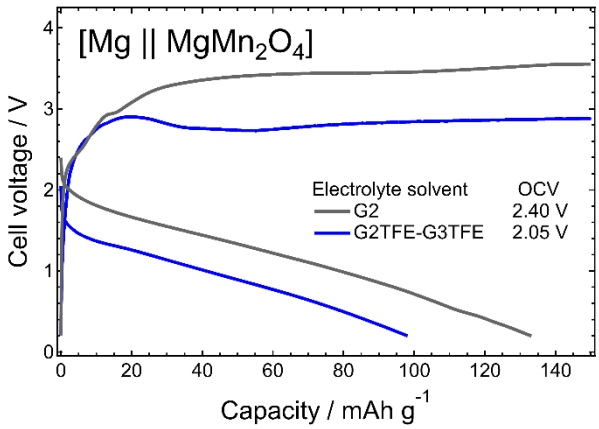

Figure 7. Initial discharge-charge profiles of [Mg || $MgMn_2O_4$] cells using the $Mg[Al(HFIP)_4]_2$/G2 and $Mg[Al(HFIP)_4]_2$/G2TFE-G3TFE electrolytes.

Recently, surface chemical treatment is attracted significant attention as an emerging technique for modifying the chemical nature of magnesium metal. By applying appropriate pre-treatment, the electrochemical activity of such magnesium metals has significantly been improved in certain modestly active electrolytes, such as halide-free ethereal solutions of $Mg[TFSA]_2$.[57–61] As well as the [anode | electrolyte] interfaces, the interfacial modification approaches have also been proposed for the [cathode | electrolyte] interfaces in the RMB research fields to mitigate the undesired side reactions by highly active transition metal oxides.[62,63] Although the strong binding of Mg^{2+} by oxide lattice would be a major cause of the failure of the oxide-based cathodes, appropriate compositional, morphological, and interfacial engineering will solve such bottleneck issues for high voltage RMB materialization.

Conclusions

In this study, we conducted systematic investigations on electrolyte solvents for RMB applications to understand the compatibility of organic solvents with magnesium metal anodes again. To avoid uncertainty derived from unambiguous side reactions of magnesium metal with electrolyte components, we used $Mg[Z(HFIP)_4]_2$ as stable conducting salts. Through the comprehensive and systematic solvent survey assisted by computational predictions, we found that solvents with intrinsic electrochemical/chemical stabilities against magnesium metal anodes and well-balanced solvating abilities are necessary to achieve the desired functionalities. Since glyme architecture was reconfirmed to be a suitable solvent design with respect to the above requirements, the improvement of the anodic stability of glyme-based solvents was investigated by minor structural modification. The substitution of the terminal methyl groups of glyme molecules by the appropriate trifluoroalkyl groups successfully imparted improved anodic stability without seriously spoiling the favorable properties of parent glymes. Certain fluorinated-glyme analogs-based electrolytes supported electrochemical magnesium deposition/dissolution activity and excellent anodic stability on Pt working electrodes. However, the applications of such fluorinated electrolytes in RMBs employing high-voltage oxide-based $MgMn_2O_4$ cathodes have failed. The subsequent chemical and electrochemical analyses revealed that side reactions between the fluorinated electrolytes and magnesium metal would occur, though relatively pure crystalline magnesium could be deposited from the same electrolytes. Such side reactions induced unfavorable passivation of magnesium anodes, resulting in a significant positive shift of the electrode potential of the anodes, consequently leading to inferior battery performances, including working voltage and discharge capacities. The instability of the fluorinated electrolytes against oxide-based cathodes also causes the failure of battery cycling.

Therefore, to realize high-energy density RMBs, it is necessary to develop highly efficient electrolytes with a sufficient electrochemical stability window. The anodic stability of these fluorinated electrolytes was remarkably enhanced compared to that of the non-fluorinated counterpart. However, the enhancement of anodic stability can lead to a reduction in cathodic stability, resulting in

a potential shift in the electrochemical stability window by a chemical modification that is unfavorable for achieving electrolyte solutions that allow reversible magnesium electrochemistry and possess sufficient anodic/chemical stabilities. To avoid this complicated situation, it is important to develop rational design concepts for feasible electrolyte solvents that consider both electrochemical (cathodic and anodic) and chemical (against both magnesium metal and prospect cathode materials) stabilities. In addition to the solvent approaches as described, the chemical/physical modification of electrode materials, including the interfacial kinetics, may also be effective in mitigating unfavorable interfacial reactions.

CRediT authorship contribution statement

Toshihiko Mandai: Conceptualization, Data curation, Formal analysis, Funding acquisition, Investigation, Project administration, Resources, Validation, Writing–original draft and review & editing. Masaru Yao: Conceptualization, Investigation, Resources, Formal analysis, Writing–review & editing. Keitaro Sodeyama: Data curation, Formal analysis, Writing–review & editing. Akiko Kagatsume: Data curation, Formal analysis, Writing–review & editing. Yoshitaka Tateyama: Data curation, Formal analysis, Writing–review & editing. Hiroaki Imai: Resources, Validation, Writing–review & editing.

Conflict of Interests

There is no conflict of interests to declare.

Supporting Information

Oxidation and reduction energies of the fluorinated glyme analogues and anions (Table S1); NMR spectra of the synthesized G*n*TFE and G*n*TFP (Figures S1–S4); CV profiles of a series of electrolyte solutions incorporating $Mg[B(HFIP)_4]_2$ (Figures S5–S8); ionic conductivities of the

selected electrolyte solutions (Figure S9); CV profiles of $Mg[Al(HFIP)_4]_2$/EiPS (Figure S10) and $Mg[B(HFIP)_4]_2$/ethyl methyl sulfone-G2 (Figure S11); molecular structures of fluorinated and sulfonated glyme analogues (Figure S12); CV profiles of $Mg[B(HFIP)_4]_2$ dissolved in G5-S2 (Figure S13) and G2TFP (Figure S14); digital images of $Mg[B(HFIP)_4]_2$ salt and its G2TFE solution (Figure S15); CV profiles of $Mg[Al(HFIP)_4]_2$/G*n*TFE (Figure S16); ionic conductivities of $Mg[Al(HFIP)_4]_2$/G*n* and $Mg[Al(HFIP)_4]_2$/G*n*TFE (Figure S17); discharge-charge profiles of [Mg | $Mg[Al(HFIP)_4]_2$/G*n*TFE | $MgMn_2O_4$] cells using three-electrode setup (Figure S18); chronoamperograms of $MgMn_2O_4$ in $Mg[Al(HFIP)_4]_2$/G*n*TFE (Figure S19).

Acknowledgments

This work was financially supported by the Advanced Low-Carbon Technology-Specially Promoted Research for Innovative Next Generation Batteries Program (ALCA-SPRING, Grant Number JPMJAL1301), the NEXT Center of Innovation Program (COI-NEXT, Grant Number JPMJPF2016), and Mirai Program (Grant Number JPMJMI20G4) of the Japan Science and Technology Agency, and Grant-in-Aid for Scientific Research (KAKENHI, 21K05263) of Japan Society for the Promotion of Science. It was also supported in part by MEXT as "Program for Promoting Researches on the Supercomputer Fugaku" (Fugaku Battery & Fuel Cell Project, Grant Number JPMXP1020200301). This research used the computational resources of supercomputers at NIMS and Fugaku through the HPCI System Research Project (project IDs: hp200131 and hp210173). The authors are also grateful for the kind support on SEM observations and XPS measurements at the NIMS Battery Research Platform.

References

1. Zhang, H.; Qiao, L.; Kühnle, H.; Figgemeier, E.; Armand, M.; Eshetu, G. G. From lithium to emerging mono- and multivalent cation-based rechargeable batteries: non-aqueous organic electrolyte and interphase perspectives. *Energy Environ. Sci*. **2023**, *16*, 11−52.
2. Ma, Z.; MacFarlane, D. R.; Kar, M. Mg Cathode Materials and Electrolytes for Rechargeable Mg Batteries: A Review. *Batteries & Supercaps* **2019**, *2*, 115–127.
3. Matsui, M. Study on electrochemically deposited Mg metal. *J. Power Sources* **2011**, *196*, 7048–7055.
4. Ghazi, Z. A.; Sun, Z.; Sun, C.; Qi, F.; An, B.; Li, F.; Cheng, H.-M. Key Aspects of Lithium Metal Anodes for Lithium Metal Batteries. *Small* **2019**, *15*, 1900687.
5. Ke, X.; Wang, Y.; Dai, L.; Yuan, C. Cell failures of all-solid-state lithium metal batteries with inorganic solid electrolytes: Lithium dendrites. *Energy Storage Mater*. **2020**, *33*, 309–328.
6. Liu, T.; Vivek, J. P.; Zhao, E. W.; Lei, J.; Araez, N. G.; Grey, C. P. Current Challenges and Routes Forward for Nonaqueous Lithium–Air Batteries. *Chem. Rev*. **2020**, *120*, 6558–6625
7. Manthiram, A.; Fu, Y.; Chung, S.-H.; Zu, C.; Su, Y.-S. Rechargeable Lithium–Sulfur Batteries. *Chem. Rev*. **2014**, *114*, 11751–11787
8. Zhang, L.; Zhao, C.; Jian, Q.; Wu, M.; Zhao, T. A high-performance lithiated silicon–sulfur battery with pomegranate-structured electrodes. *J. Power Sources* **2021**, *506*, 230174
9. Liu, Y.; Wei, H.; Zhai, X.; Wang, F.; Ren, X.; Xiong, Y.; Akiyoshi, O.; Pan, K.; Ren, F.; Wei, S. Graphene-based interlayer for high-performance lithium–sulfur batteries: A review. *Mater. Des*. **2021**, *211*, 110171.
10. Shiga, T.; Hase, Y.; Kato, Y.; Inoue, M.; Takechi, K. A rechargeable non-aqueous Mg–O_2 battery. *Chem. Commun*., **2013**, *49*, 9152–9154.
11. Kim, H. S.; Arthur, T. S.; Allred, G. D.; Zajicek, J.; Newman, J. G.; Rodnyansky, A. E.; Oliver, A. G.; Boggess, W. C.; Muldoon, J. Structure and compatibility of a magnesium electrolyte with a sulphur cathode. *Nat. Commun*. **2011**, *2*, 427.
12. Zhao-Kerger, Z.; Liu, R.; Dai, W.; Li, Z.; Diemant, T.; Vinayan, B. P.; Minella, C. B.; Yu, X.; Manthiram, A.; Behm, R. J.; et al. Toward Highly Reversible Magnesium−Sulfur Batteries with Efficient and Practical $Mg[B(hfip)_4]_2$ Electrolyte. *ACS Energy Lett*. **2018**, *3*, 2005–2013.
13. Tan, S.; Xiong, F.; Wang, J.; An, W.; Mai, L. Crystal regulation towards rechargeable magnesium battery cathode materials. *Mater. Horiz*. **2020**, *7*, 1971–1995.
14. Li, L.; Lu, Y.; Zhang, Q.; Zhao, S.; Hu, Z.; Chou, S.-L. Recent Progress on Layered Cathode Materials for Nonaqueous Rechargeable Magnesium Batteries. *Small* **2019**, 1902767.
15. Ue, M.; Sakaushi, K.; Uosaki, K. Basic knowledge in battery research bridging the gap between academia and industry. *Mater. Horiz*. **2020**, *7*, 1937–1954.
16. Lu, Z.; Schechter, A.; Moshkovich, M.; Aurbach, D. On the electrochemical behavior of magnesium electrodes in polar aprotic electrolyte solutions. *J. Electroanal. Chem*. **1999**, *466*, 203–217.
17. Gregory, T. D.; Hoffman, R. J.; Winterton, R. C. Nonaqueous Electrochemistry of Magnesium: Applications to Energy Storage. *J. Electrochem. Soc*. **1990**, *137*, 775–780.
18. Ha, S.-Y.; Lee, Y.-W.; Woo, S. W.; Koo, B.; Kim, J.-S.; Cho, J.; Lee, K. T.; Choi, N.-S. Magnesium(II) Bis(trifluoromethane sulfonyl) Imide-Based Electrolytes with Wide

Electrochemical Windows for Rechargeable Magnesium Batteries. *ACS Appl. Mater. Interfaces* **2014**, *6*, 4063−4073.

19. Orikasa, Y.; Masese, T.; Koyama, Y.; Mori, T.; Hattori, M.; Yamamoto, K.; Okado, T.; Huang, Z.-D.; Minato, T.; Tassel, C.; et al. High energy density rechargeable magnesium battery using earth-abundant and non-toxic elements. *Sci. Rep*. **2014**, *4*, 5622.
20. Shterenberg, I.; Salama, M,; Yoo, H. D.; Gofer, Y.; Park, J.-B.; Sun, Y.-K.; Aurbach, D. Evaluation of $(CF_3SO_2)_2N^-$ (TFSI) Based Electrolyte Solutions for Mg Batteries. *J. Electrochem. Soc*. **2015**, *162*, A7118–A7128.
21. Sa, N.; Pan, B.; Shah, A. S.; Hubaud, A. A.; Vaughey, J. T.; Baker, L. A.; Liao, C.; Burrell, A. K. Role of Chloride for a Simple, Non-Grignard Mg Electrolyte in Ether-Based Solvents. *ACS Appl. Mater. Interfaces* **2016**, *8*, 16002−16008.
22. Muldoon, J.; Bucur, C. B.; Oliver, A. G.; Zajicek, J.; Allred, G. D.; Boggess, W. C. Corrosion of magnesium electrolytes: chlorides – the culprit. *Energy Environ. Sci*. **2013**, *6*, 482–487
23. Mandai, T.; Tatesaka, K.; Soh, K.; Masu, H.; Choudhary, A.; Tateyama, Y.; Ise, R.; Imai, H.; Takeguchi, T.; Kanamura, K. Modifications in coordination structure of $Mg[TFSA]_2$-based supporting salts for high-voltage magnesium rechargeable batteries. *Phys. Chem. Chem. Phys*. **2019**, *21*, 12100–12111.
24. Kang, S. J.; Lim, S.-C.; Kim, H.; Heo, J. W.; Hwang, S.; Jang, M.; Yang, D.; Hong, S.-T.; Lee, H. Non-Grignard and Lewis Acid-Free Sulfone Electrolytes for Rechargeable Magnesium Batteries. *Chem. Mater*. **2017**, *29*, 3174−3180.
25. Hou, S.; Ji, X.; Gaskell, K.; Wang, P.; Wang, L.; Xu, J.; Sun, R.; Borodin, O.; Wang, C. Solvation sheath reorganization enables divalent metal batteries with fast interfacial charge transfer kinetics. *Science* **2021**, *374*, 172–178.
26. Fan, S.; Asselin, G. M.; Pan, B.; Wang, H.; Ren, Y.; Vaughey, J. T.; Sa, N. A Simple Halogen-Free Magnesium Electrolyte for Reversible Magnesium Deposition through Cosolvent Assistance. *ACS Appl. Mater. Interfaces* **2020**, *12*, 10252−10260.
27. Zhao, W.; Pan, Z.; Zhang, Y.; Liu, Y.; Dou, H.; Shi, X.; Zuo, Z.; Zhang, B.; Chen, J.; Zhao, X.; et al. Tailoring Coordination in Conventional Ether-Based Electrolytes for Reversible Magnesium-Metal Anodes. *Angew. Chem. Int. Ed*. **2022**, *61*, e202205187.
28. Son, S.-B.; Gao, T.; Harvey, S. P.; Steirer, K. X.; Stokes, A.; Norman, A.; Wang, C.; Cresce, A.; Xu, K.; Ban, C. An artificial interphase enables reversible magnesium chemistry in carbonate electrolytes. *Nat. Chem*. **2018**, *10*, 532−539.
29. Mandai, T. Critical Issues of Fluorinated Alkoxyborate–Based Electrolytes in Magnesium Battery Applications. *ACS Appl. Mater. Interface* **2020**, *12*, 39135–39144.
30. Mandai, T.; Youn, Y.; Tateyama, Y. Remarkable electrochemical and ion-transport characteristics of magnesium-fluorinated alkoxyaluminate–diglyme electrolytes for magnesium batteries. *Mater. Adv*. **2021**, *2*, 6283–6296.
31. Mandai, T.; Yoshida, K.; Tsuzuki, S.; Nozawa, R.; Masu, H.; Ueno, K.; Dokko, K.; Watanabe, M. Effect of Ionic Size on Solvate Stability of Glyme-Based Solvate Ionic Liquids. *J. Phys. Chem. B* **2015**, *119*, 1523−1534.

32. Amanchukwu, C. V.; Yu, Z.; Kong, X.; Qin, J.; Cui, Y.; Bao, Z. A New Class of Ionically Conducting Fluorinated Ether Electrolytes with High Electrochemical Stability. *J. Am. Chem. Soc*. **2020**, *142*, 7393−7403.
33. Liu, J.-B.; Chen, C.; Chu, L.; Chen, Z.-H.; Xu, X.-H.; Qing, F.-L. Silver-Mediated Oxidative Trifluoromethylation of Phenols: Direct Synthesis of Aryl Trifluoromethyl Ethers. *Angew. Chem. Int. Ed*. **2015**, *54*, 11839−11842.
34. Mandai, T.; Akita, Y.; Yagi, S.; Egashira, M.; Munakata, H.; Kanamura, K. A key concept of utilization of both non-Grignard magnesium chloride and imide salts for rechargeable Mg battery electrolytes. *J. Mater. Chem. A* **2017**, *5*, 3152–3156.
35. Mandai, T.; Somakwa, H. Ultrathin Magnesium Metal Anode – An Essential Component for High-Energy-Density Magnesium Battery Materialization. *Batteries & Supercaps* **2022**, *5*, e202200153.
36. Sone, K.; Hayashi, Y.; Mandai, T.; Yagi, S.; Oaki, Y.; Imai, H. Effective 3D open-channel nanostructures of a $MgMn_2O_4$ positive electrode for rechargeable Mg batteries operated at room temperature. *J. Mater. Chem. A* **2021**, *9*, 6851–6860.
37. Frisch, M. J. et al., Revision C.01, Gaussian Inc., Wallingford CT, 2019
38. Marenich, A. V.; Cramer, C. J.; Truhlar, D. G. Universal solvation model based on solute electron density and on a continuum model of the solvent defined by the bulk dielectric constant and atomic surface tensions. *J. Phys. Chem. B* **2009**, *113*, 6378–6396.
39. Herb, J. T.; Nist-Lund, C. A.; Arnold, C. B. A Fluorinated Alkoxyaluminate Electrolyte for Magnesium-Ion Batteries. *ACS Energy Lett*. **2016**, *1*, 1227–1232.
40. Zhao-Karger, Z.; Bardaji, M. E. G.; Fuhr, O.; Fichtner, M. A new class of non-corrosive, highly efficient electrolytes for rechargeable magnesium batteries. *J. Mater. Chem. A* **2017**, *5*, 10815–10820.
41. Shterenberg, I.; Salama, M.; Gofer, Y.; Aurbach, D. Hexafluorophosphate-Based Solutions for Mg Batteries and the Importance of Chlorides. *Langmuir* **2017**, *33*, 9472–9478.
42. Yu, Z.; Wang, H.; Kong, X.; Huang, W.; Tsao, Y.; Mackanic, D. G.; Wang, K.; Wang, X.; Huang, W.; Choudhury, S.; et al. Molecular design for electrolyte solvents enabling energy-dense and long-cycling lithium metal batteries. *Nat. Energy* **2020**, *5*, 526–533.
43. Dhattarwal, H. S.; Kuo, J.-L.; Kashyap, H. K. Mechanistic Insight on the Stability of Ether and Fluorinated Ether Solvent-Based Lithium Bis(fluoromethanesulfonyl) Electrolytes near Li Metal Surface. *J. Phys. Chem. C* **2022**, *126*, 8953–8963.
44. Peljo, P.; Girault, H. H. Electrochemical potential window of battery electrolytes: the HOMO–LUMO misconception. *Energy Environ. Sci*. **2018**, *11*, 2306–2309
45. Lautar, A. K.; Bitenc, J.; Rejec, T.; Dominko, R.; Filhol, J.-S.; Doublet, M.-L. Electrolyte Reactivity in the Double Layer in Mg Batteries: An Interface Potential-Dependent DFT Study. *J. Am. Chem. Soc*. **2020**, *142*, 5146–5153.
46. Strasser, S.; Slugovc, C. Nucleophile-mediated oxa-Michael addition reactions of divinyl sulfone – a thiol-free option for step-growth polymerisations. *Catal. Sci. Technol*. **2015**, *5*, 5091–5094.
47. Ren, W.; Wu, D.; NuLi, Y.; Zhang, D.; Yang, Y.; Wang, Y.; Yang, J.; Wang, J. An Efficient Bulky $Mg[B(Otfe)_4]_2$ Electrolyte and Its Derivatively General Design Strategy for Rechargeable Magnesium Batteries. *ACS Energy Lett*. **2021**, *6*, 3212−3220.

48. Xie, X.; Leon, N. J.; Small, D. W.; Smith, E. W. C. S.; Liao, C.; Persson, K. A. Reductive Decomposition Kinetics and Thermodynamics That Govern the Design of Fluorinated Alkoxyaluminate/Borate Salts for Mg-Ion and Ca-Ion Batteries. *J. Phys. Chem. C* **2022**, *126*, 20773−20785.
49. Jankowski, P.; Li, Z.; Karger, Z. Z.; Diemant, T.; Fichtner, M.; Vegge, T.; Lastra, J. M. G. Development of Magnesium Borate Electrolytes: Explaining the Success of $Mg[B(hfip)_4]_2$ Salt. *Energy Storage Mater*. **2022**, *45*, 1133–1143.
50. Pavčnik, T.; Lozinšek, M.; Pirnat, K.; Vizintin, A.; Mandai, T.; Aurbach, D.; Dominko, R.; Bitenc, J. On the Practical Applications of the Magnesium Fluorinated Alkoxyaluminate Electrolyte in Mg Battery Cells. *ACS Appl. Mater. Interfaces* **2022**, *14*, 26766−26774.
51. Gatto, V. J.; Arnold, K. A.; Viscariello, A. M.; Miller, S. R.; Morgan, C. R.; Gokel, G. W. Syntheses and Binding Properties of Bibracchial Lariat Ethers (BiBLEs): Survey of Synthetic Methods and Cation Selectivities. *J. Org. Chem*. **1986**, *51*, 5373−5384.
52. Aurbach, D.; Gofer, Y. *The Electrochemical Window of Nonaqueous Electrolyte Solutions. In Nonaqueous Electrochemistry*; Aurbach, D., Ed.; Marcel Dekker: New York, 1999; pp 137−212.
53. Zhang, X.; Winget, B.; Doeff, M.; Evans, J. W.; Devine, T. M. Corrosion of Aluminum Current Collectors in Lithium-Ion Batteries with Electrolytes Containing $LiPF_6$. *J. Electrochem. Soc*. **2005**, *152*, B448−B454.
54. Kramer, E.; Schedlbauer, T.; Hoffmann, B.; Terborg, L.; Nowak, S.; Gores, H. J.; Passerini, S.; Winter, M. Mechanism of Anodic Dissolution of the Aluminum Current Collector in 1 M LiTFSI EC:DEC 3:7 in Rechargeable Lithium Batteries. *J. Electrochem. Soc*. **2013**, *160*, A356–A360.
55. Xu, S.; Luo, G.; Jacobs, R.; Fang, S.; Mahanthappa, M. K.; Hamers, R. J.; Morgan, D. Ab Initio Modeling of Electrolyte Molecule Ethylene Carbonate Decomposition Reaction on $Li(Ni,Mn,Co)O_2$ Cathode Surface. *ACS Appl. Mater. Interfaces* **2017**, *9*, 20545−20553.
56. Lim, G.; Shin, D.; Chae, K. H.; Cho, M. K.; Kim, C.; Sohn, S. S.; Lee, M.; Hong, J. Regulating Dynamic Electrochemical Interface of $LiNi_{0.5}Mn_{1.5}O_4$ Spinel Cathode for Realizing Simultaneous Mn and Ni Redox in Rechargeable Lithium Batteries. *Adv. Energy Mater*. **2022**, *12*, 2202049.
57. Zhang, J.; Guan, X.; Lv, R.; Wang, D.; Liu, P.; Luo, J. Rechargeable Mg metal batteries enabled by a protection layer formed in vivo. *Energy Storage Mater*. **2020**, *26*, 408–413.
58. Lv, R.; Guan, X.; Zhang, J.; Xia, Y.; Luo, J. Enabling Mg metal anodes rechargeable in conventional electrolytes by fast ionic transport interphase. *Natl. Sci. Rev*. **2020**, *7*, 333–341
59. Li, Y.; Zuo, P.; Li, R.; Huo, H.; Ma, Y.; Du, C.; Gao, Y.; Yin, G.; Weatherup, R. S. Formation of an Artificial Mg^{2+}-Permeable Interphase on Mg Anodes Compatible with Ether and Carbonate Electrolytes. *ACS Appl. Mater. Interfaces* **2021**, *13*, 24565−24574.
60. Zhao, Y.; Du, A.; Dong, S.; Jiang, F.; Guo, F.; Ge, X.; Qu, X.; Zhou, X.; Cui, G. A Bismuth-Based Protective Layer for Magnesium Metal Anode in Noncorrosive Electrolytes. *ACS Energy Lett*. **2021**, *6*, 2594–2601.
61. Bae, J.; Park, H.; Guo, X.; Zhang, X.; Warner, J. H.; Yu, G. High-performance magnesium metal batteries via switching the passivation film into a solid electrolyte interphase. *Energy Environ. Sci*. **2021**, *14*, 4391–4399.

62. Doi, S.; Ise, R.; Mandai, T.; Oaki, Y.; Yagi, S.; Imai, H. Spinel-Type $MgMn_2O_4$ Nanoplates with Vanadate Coating for a Positive Electrode of Magnesium Rechargeable Batteries. *Langmuir* **2020**, *36*, 8537−8542.
63. Kajihara, K.; Takahashi, D.; Kobayashi, H.; Mandai, T.; Imai, H.; Kanamura, K. Phenylphosphonate surface functionalisation of $MgMn_2O_4$ with 3D open-channel nanostructures for composite slurry-coated cathodes of rechargeable magnesium batteries operated at room temperature. *RSC Adv.* **2021**, *11*, 19076–19082.

TOC graphic

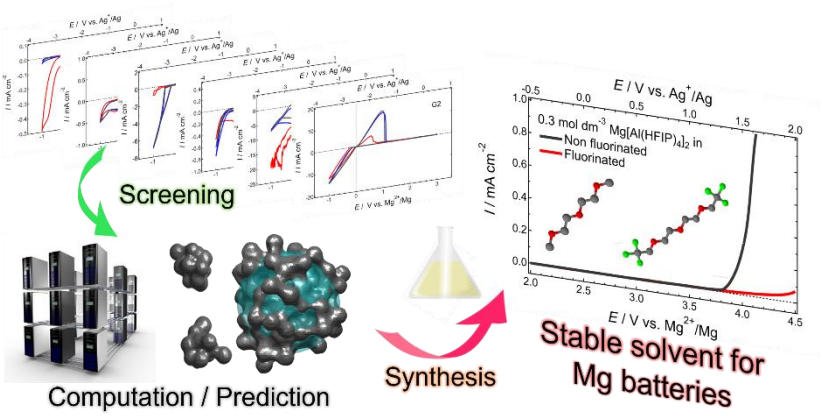
Screening
Computation / Prediction
Synthesis
E / V vs. Ag+/Ag
0.3 mol dm-3 Mg[Al(HFIP)4]2 in
Non fluorinated
Fluorinated
I / mA cm-2
E / V vs. Mg2+/Mg
Stable solvent for
Mg batteries